Numerical Modeling of Flow Through Phloem Considering Active Loading

Tsun-kay Jackie Sze

Jin Liu

Prashanta Dutta[1]
e-mail: dutta@mail.wsu.edu

School of Mechanical and Materials Engineering,
Washington State University,
Pullman, WA 99164

Transport through phloem is of significant interest in engineering applications, including self-powered microfluidic pumps. In this paper we present a phloem model, combining protein level mechanics with cellular level fluid transport. Fluid flow and sucrose transport through a petiole sieve tube are simulated using the Nernst–Planck, Navier–Stokes, and continuity equations. The governing equations are solved, using the finite volume method with collocated storage, for dynamically calculated boundary conditions. A sieve tube cell structure consisting of sieve plates is included in a two dimensional model by computational cell blocking. Sucrose transport is incorporated as a boundary condition through a six-state model, bringing in active loading mechanisms, taking into consideration their physical plant properties. The effects of reaction rates and leaf sucrose concentration are investigated to understand the transport mechanism in petiole sieve tubes. The numerical results show that increasing forward reactions of the proton sucrose transporter significantly promotes the pumping ability. A lower leaf sieve sucrose concentration results in a lower wall inflow velocity, but yields a higher inflow of water due to the active loading mechanism. The overall effect is a higher outflow velocity for the lower leaf sieve sucrose concentration because the increase in inflow velocity outweighs the wall velocity. This new phloem model provides new insights on mechanisms which are potentially useful for fluidic pumping in self-powered microfluidic pumps.
[DOI: 10.1115/1.4025869]

Keywords: proton sucrose transporter, flow through phloem, finite volume, micropump

1 Introduction

Micropumps are of significant importance in microfluidic devices due to their applications in drug delivery, environmental monitoring, lab-on-a-chip analysis, power generation, and printing [1,2]. Micropumps can be categorized into two types: mechanical and nonmechanical [2]. Mechanical micropumps utilize either a syringe, diaphragm, or gear to convert external mechanical energy into flow energy. Mechanical micropumps have many disadvantages, including pulsating flow, bulky size, complex integration issue, and incompatibility with biological fluids. To circumvent the aforementioned shortcomings, nonmechanical pumping methods have been proposed, such as electrohydrodynamic and magnetohydrodynamic micropumps [2]. However, these nonmechanical micropumps also have issues such as they require large supporting systems, have limited fluid compatibility, and cause Joule heating. Joule heating results in high temperatures, which can destroy biological cells, DNA, or proteins [3,4]. Many of these nonmechanical methods such as electrostatic and electrohydrodynamic micropumps require high voltage, which has the drawback of forming gasses, potentially clogging the tiny channels in microdevices [5]. Additionally, most microfluidic devices are made to be disposable; thus, including complex components such as valves, heaters, and actuators are undesirable due to added cost [6].

Biological systems have long been of interest for scientists in search of phenomenon to apply in engineering systems. Scientists have applied Characean cells for mixing, shark skin for drag reduction, artificial leaves to extract water, and sucrose transporters to actuate [7,8]. The sucrose transporter proteins from phloem have been shown to be capable of generating enough fluid displacement to deform the cover plate of an actuator.

Plants are capable of self-sustained pumping; where nutrients are transported from sources such as leaves through stems to sinks (see Fig. 1(*a*)), including roots and fruits without external pressure or power. Nutrients such as sugars are transported through vascular networks called phloem built up by cells, including sieve elements for fluid transport, parenchyma cells with specialized companion cells for sieve biological support, and additional structural supporting cells. Sieve elements are interconnected with sieve plates containing pores that allow fluids to pass through, as shown in Fig. 1(*b*). These sieve cells have typical diameters from 1–40 μm with flow velocities from 3–300 μm/s. These ranges come within microfluidic operation ranges; hence, understanding fluid flow in plants is of significant interest for microfluidic devices.

Fluid transport in plants is a very complex phenomenon and many approaches have been used to model this mechanism. An entire section of a plant may be modeled as a bulk using a series of resistances to represent mass transport in different plant segments with different resistances. This method has been applied to plants to simulate the entire trunks to study flow in both xylem and phloem [9,10]. While being robust and incorporating the entire trunk, these methods require that the flow resistance be known beforehand.

Alternately, there are sieve tube oriented models, which focus on the mechanics in the phloem. A comprehensive overview of early models has been covered by Thompson and Holbrook [11]. Many simplified phloem models are developed based on simple tube flow by ignoring the effect of sieve plates using Hagen–Poiseuille approximations. However, pressure distribution in a sieve tube without any resisting/sieve plates will be significantly different. In the presence of a sieve plate the fluid flow resistance may be eight times higher than those of simple tube models [11]. More advanced numerical works on flow through phloem used a quasi 1D approach by solving mass conservation equation. In those works, wall mass flux is used to bring pressure into the governing equation and pressure drops inside the sieve tube and sieve plates are calculated based on various assumptions. For instance, Christy

[1]Corresponding author.

Contributed by the Fluids Engineering Division of ASME for publication in the Journal of Fluids Engineering. Manuscript received August 1, 2013; final manuscript received October 4, 2013; published online December 12, 2013. Assoc. Editor: Ali Beskok.

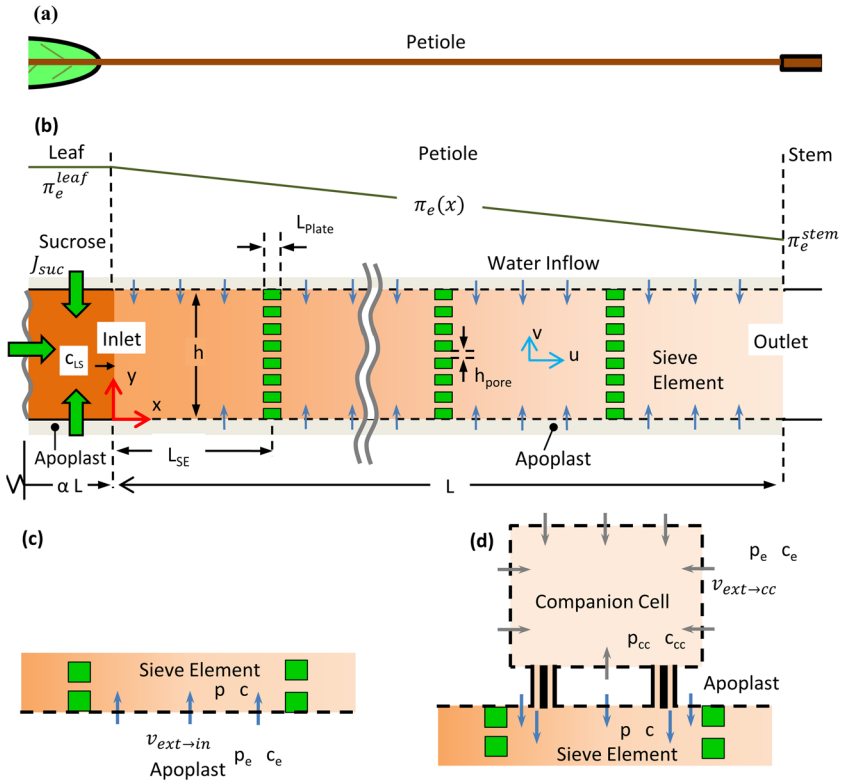

Fig. 1 (*a*) Schematic of a petiole section connecting the leaf to the stem. (*b*) Computational domain and associated boundary conditions for flow through a sieve tube. Schematic of flow penetration from the (*c*) bottom, and (*d*) top surfaces. For the bottom wall, water enters directly into the sieve. While for the top wall, in addition to entering directly, water will also first enter into the neighboring companion cell and then into the sieve tube.

and Ferrier [12] considered the flow resistance in the sieve plate by calculating pressure drops through pores. Thompson and Holbrook [11] considered the Dagan pressure drop, which are losses in pores located in an infinitely wide plate, to calculate the flow resistance in the sieve plate. However, these models do not consider the effects of neighboring pores. To better understand the effect of sieve plates, numerical simulations of fluid flow over sieve plates have been attempted [13,14]. However, these studies did not consider the water flow through walls and the transport of solutes through the sieve tube.

Another important aspect of transport in phloem is sugar influx mechanisms. One primary route plants use to load sugars into sieve tubes is through active loading by use of specialized sucrose transporter proteins (STPs). Active loading is of significant interest since it allows for reduced leaf sucrose concentrations with potential advantages, including less vulnerability to predators, faster leaf growth, and less inhibition of photosynthesis due to sugar buildup [15]. In a recent study, De Schepper et al. [10] provided active loading mechanisms in their tree model using Michaelis–Menten kinetics [16] with the sucrose influx dependency based on external sucrose concentrations. In reality, proton concentrations and membrane electric potentials also affect sucrose influx [17]. However, to our knowledge, no study has included proton dependent sucrose transport through phloem.

In this study we present flow through phloem, considering active transport of sucrose via STPs using a 6-state sucrose transporter model. We are primarily interested in self-sustained fluid pumping mechanisms in plants. Thus, we study flow through sieve tubes by including the active mechanics of sucrose influx in the system considering the proton, sucrose, and electric potential both inside and outside of the leaf sieve tube. The rest of the paper is organized as follows. In Sec. 2, we describe transport through the petiole sieve tube using relevant governing equations and boundary conditions. In Sec. 3 the incorporation of leaf sucrose influx into leaf sieve tubes is presented using a 6-state sucrose transporter model. The development of the numerical model is presented in Sec. 4. All physical and chemical properties used in this study are shown in Sec. 5. Section 6 presents the verification steps taken for our numerical methods. We present our results and conclusions in Secs. 7 and 8, respectively.

2 Flow Through Phloem

Plant cell membranes have specialized channels called aquaporins that allow the passage of small neutral molecules such as water, but prevent ions and larger molecules such as sugars from passing [18]. Hence, the cell membrane can be seen as semipermeable, allowing the transport of water. Outside of the cell membrane is the apoplast, which includes the interconnected space in between live cells allowing water and solutes to move freely (see Fig. 1(*b*)).

Phloem in plants operates under osmotic pumping principles, where sugar and water are transported through sieve tubes. In a plant the sugar concentration is higher inside a sieve tube than the surrounding apoplast. Thus the osmotic pressure is higher inside the sieve tube and the osmotic pressure difference will facilitate the water transport from apoplast to the sieve tube. In order to have a higher sugar concentration inside the sieve tube, sugar molecules must be continuously pumped inside the sieve tubes. In a plant leaf section, sugars and ions are actively loaded in the sieve tube through a proton gradient and negative membrane electric potential between the sieve and apoplast.

2.1 Mathematical Model. We model the petiole of a plant connecting a leaf, where the sugar is loaded, to the stem of the plant, as shown in Fig. 1(*a*). We consider the Solanaceae plant family; this plant family covers plants such as eggplant, potato,

tobacco, and tomato [19]. To model flow through petiole sieve tubes, we consider the transport of sucrose in a 2D channel consisting of a chain of sieve elements with porous sieve plates, as shown in Fig. 1(*b*). We represent the petiole sieve tube wall as a semipermeable cell membrane; permeable to water but not sucrose.

Sugar is produced in the leaves by photosynthesis and transported into leaf sieve tubes by STPs using active loading, which then enters the petiole sieve elements. Water can enter petiole sieve elements both directly and indirectly. In the direct case, water enters due to the pressure difference, as shown in Fig. 1(*c*). In the indirect case, water first enters neighboring companion cells and then the sieve elements, as depicted in Fig. 1(*d*). These companion cells are connected with petiole sieves by plasmodesmata. The geometry of plasmodesmata is still under debate, but for this work we represent plasmodesmata as an annular pore and the companion cells are assumed to be on one side (upper) of the petiole sieve tube.

2.2 Governing Equations. To compute the flow through the petiole sieve tube, we develop a mathematical model based on the steady state Nernst–Planck, Navier–Stokes, and continuity equations. We model the fluid, also known as sap, in the sieve tube as a sucrose water solution. The transport of sucrose is governed by the Nernst–Planck equation [20]. Since sucrose is electrically neutral, we drop the electromigration term; hence, the Nernst–Planck equation simplifies to

$$\frac{\partial}{\partial x}(uc)+\frac{\partial}{\partial y}(vc)=\frac{\partial}{\partial x}\left(D\frac{\partial c}{\partial x}\right)+\frac{\partial}{\partial y}\left(D\frac{\partial c}{\partial y}\right) \tag{1}$$

If we assume that the fluid is incompressible, the flow will be governed by the continuity and the Navier–Stokes equations:

$$\frac{\partial u}{\partial x}+\frac{\partial v}{\partial y}=0 \tag{2a}$$

$$\rho u\frac{\partial u}{\partial x}+\rho v\frac{\partial u}{\partial y}=\frac{\partial}{\partial x}\left(\mu\frac{\partial u}{\partial x}\right)+\frac{\partial}{\partial y}\left(\mu\frac{\partial u}{\partial y}\right)-\frac{\partial p}{\partial x} \tag{2b}$$

$$\rho u\frac{\partial v}{\partial x}+\rho v\frac{\partial v}{\partial y}=\frac{\partial}{\partial x}\left(\mu\frac{\partial v}{\partial x}\right)+\frac{\partial}{\partial y}\left(\mu\frac{\partial v}{\partial y}\right)-\frac{\partial p}{\partial y} \tag{2c}$$

2.3 Boundary Conditions. We simulate flow in the petiole sieve tube, as shown in Fig. 1(*b*). For the Nernst–Planck equation, no sucrose is added or removed and a mixed boundary is used at the top and bottom surfaces

$$D\frac{\partial c}{\partial y}-vc=0 \tag{3}$$

At the outlet we consider the sucrose concentration change is negligible, hence

$$\frac{\partial c}{\partial x}=0 \tag{4}$$

At the inlet, the sucrose concentration is the same as the leaf sieve sucrose concentrations (c_{LS}) [21]. Thus, we use the Dirichlet boundary condition by setting a fixed sucrose concentration based on the leaf sieve sucrose concentration:

$$c=c_{LS} \tag{5}$$

For fluid velocities, a penetrating velocity due to the pressure difference will be specified on the top and bottom face of the petiole. The velocity across a permeable membrane can be represented using the Kedem and Katchalsky equation [22]

$$v_w=M_p[p_e-p_i-\sigma(\pi(c_e)-\pi(c_i))] \tag{6}$$

For a semipermeable membrane (impermeable to solute) σ is 1. Osmotic pressures (π) are calculated from sucrose concentrations.

On the bottom wall, there will only be wall flow from the surrounding apoplast into the petiole sieve element. Thus, we use Eq. (6) to calculate the penetrating velocity ($v_{ext\to in}$) and consider no slip velocity in the x direction. The apoplast (external) thermodynamic p_e and osmotic $\pi(c_e)$ pressures are defined based on plant values, while the sieve (internal) values are numerically calculated.

On the top wall, there will be two contributions to wall flow: from the surrounding apoplast directly into the sieve ($v_{ext\to in}$) and from the apoplast into the companion cell then into the sieve ($v_{ext\to cc\to in}$). Thus, the boundary conditions for the top wall are

$$\begin{aligned} v&=-v_{ext\to in}-v_{ext\to cc\to in}\\ u&=0 \end{aligned} \tag{7}$$

Water flow from the surrounding area follows the same process as described earlier, except that the computational cells will now be neighboring the top boundary. We represent the companion cell as a rectangular control volume with a single pressure and sucrose concentration. The companion cell is assumed to have the same internal length as the sieve and a height of $\alpha_{cc}h$. As a result the net volumetric flow per unit width Q_n into the nth companion cell will be

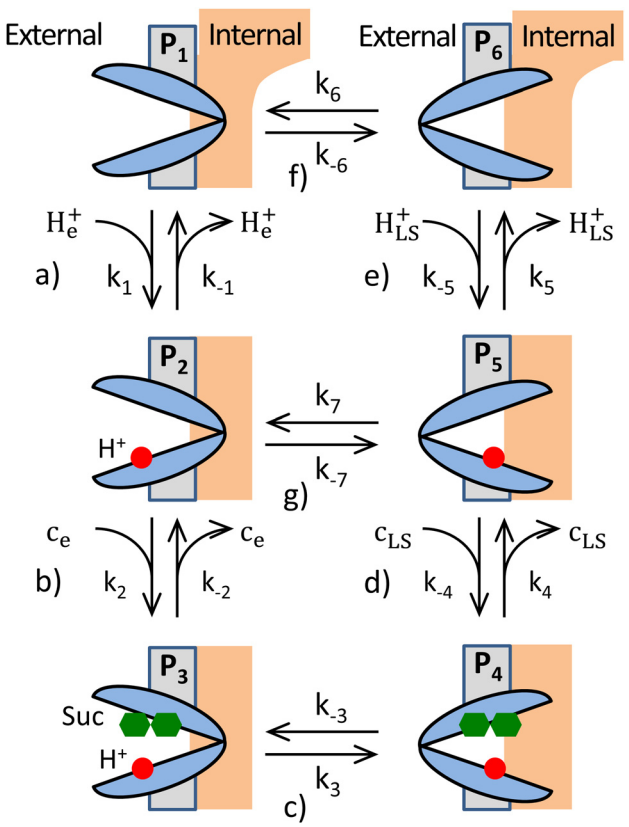

Fig. 2 Six-state model for potato STP adapted from Boorer et al. [17] for sucrose transport from outside (apoplast) to inside (leaf sieve). Each protein state is denoted as P_m ($m=1, 2,\ldots,6$). The forward reaction allows entry of sucrose into the sieve element from the apoplast. In the first state (P_1) unbounded protein is open to the outside. Transition to the second state (P_2) takes place when a proton (H^+) from outside binds to P_1. Next a sucrose molecule binds to P_2 to form P_3. This is followed by a conformational change from the protein being open to the outside to in ($P_3 \to P_4$), bringing the proton and sucrose molecule inside the leaf sieve tube. The sucrose molecule leaves P_4 to form P_5 and, finally, the proton leaves from P_5 resulting in P_6. The cycle is completed by the change in confirmation from being open inwards P_6 to outwards P_1.

$$Q_n = 2\left(L_{\mathrm{SE}} - L_{\mathrm{plate}} + \alpha_{\mathrm{cc}} h\right) M_p \left[p_e - p_{\mathrm{cc}\,n} - \left(\pi(c_e) - \pi(c_{\mathrm{cc}n})\right)\right] \tag{8}$$

Here, we assume that the nth companion cell is only connected with a neighboring nth sieve element. The sieve-averaged sucrose concentration and thermodynamic pressure p_n are found by averaging the top face of the nth sieve. The sieve-averaged sucrose concentration is used as the companion cell sucrose concentration ($c_{\mathrm{cc}\ n}$). The companion cell pressure ($p_{\mathrm{cc}\ n}$) is calculated based on the sieve pressure.

If the companion cell is isolated from all surrounding cells except the sieve element, then flow entering the companion cell must enter the sieve. Using plant plasmodesmata density (ϑ_{pl}), the fluid flow ($q_{\mathrm{pl}\ n}$) across a single plasmodesma can be determined as a function of net volumetric flow. If the loss between the companion cell and sieve is dominated by plasmodesmata restriction, then the pressure of the companion cell can be approximated using annular pore flow [23]

$$p_{\mathrm{cc}\,n} = p_n + L_{\mathrm{pl}} \left(\frac{\pi r_{\mathrm{pl}o}^4}{8\mu} \left[1 - \kappa^4 - \frac{(1-\kappa^2)^2}{\ln(1/\kappa)} \right] \right)^{-1} q_{\mathrm{pl}\,n}, \qquad \kappa = r_{\mathrm{pl}i}/r_{\mathrm{pl}o} \tag{9}$$

where the dimensions of the plasmodesmata are given by the length L_{pl}, outer radius $r_{\mathrm{pl}\ o}$, and inner radius $r_{\mathrm{pl}\ i}$. Combining Eqs. (8) and Eq. (9), we can determine the net volumetric flow into the companion cell. Using volumetric flow, the flow velocity from the companion cell to petiole sieve can be determined by dividing the volumetric flow over the wall surface area

$$v_{\mathrm{ext}\to\mathrm{cc}\to\mathrm{in}} = Q_n / \left(L_{\mathrm{SE}} - L_{\mathrm{plate}}\right) \tag{10}$$

At the inlet we consider a fully developed flow profile

$$v = 0, \qquad u(y) = \bar{u}_{\mathrm{in}} \frac{6}{h^2} \left(yh - y^2\right) \tag{11}$$

where the parabolic profile is used based on the mean inflow velocity ($\bar{u}_{\mathrm{in}}$). The inlet flow velocity is calculated from the sucrose flux (J_{suc}) as

$$\bar{u}_{\mathrm{in}} = \frac{J_{\mathrm{suc}}}{c_{\mathrm{in}}} \alpha_{\mathrm{ccL}} \frac{L\alpha}{h} \tag{12}$$

The sucrose flux J_{suc} is based on the six-state model, which is discussed later in Sec. 3. The factor α_{ccL} is included to incorporate the conversion between the transfer cell and leaf sieve surface area. At the outlet boundary we define the pressure based on sieve tube values. We also consider the outflow velocity as fully developed

$$\frac{\partial u}{\partial x} = 0, \qquad v = 0 \tag{13}$$

3 Sucrose Influx Mechanism

Key plant species such as celery, common bean, potato, tobacco, and tomato use active loading to transport sugars into sieve tubes [24]. In this section we present an explanation of the sucrose loading mechanics based on potato STPs. Active loading utilizes a proton gradient and membrane electrical potential difference to move sucrose molecules from the apoplast into the leaf sieve through STPs. Several models based on experimental measurements from cloned STPs have been proposed [17,25]. Here we adopted the more complete six-state model provided by Boorer et al. [17] for potato plants, as illustrated in Fig. 2. The six-state model represents the sucrose transporter with six individual protein states utilizing 14 forward ($\rightarrow$) and reverse ($\leftarrow$) reactions. The forward reaction rate constant is denoted as k_m, while the reverse rate is k_{-m}. The protein density at a particular state is denoted by P_m. As shown in Fig. 2, the sucrose transport flux is dependent on properties such as proton and sucrose concentrations in the apoplast and leaf sieve tube.

Based on the six-state model, sucrose fluxes representing active loading can be calculated through the use of rate equations. While the six-state model derived by Boorer et al. includes a total of 14 rates, proton slippage rates (k_7 and k_{-7}) are extremely small in comparison to other rates; therefore, we neglect the process (see Fig. 2(*g*)) in the calculation of J_{suc}.

The rate at which a particular protein state occurs can be determined from the law of mass action. For the system shown in Fig. 2, protein densities at different protein states can be given as

$$\begin{aligned}
\frac{dP_1}{dt} &= k_6 P_6 - k_{-6} P_1 + k_{-1} P_2 - k_1 P_1 H_e^+ \\
\frac{dP_2}{dt} &= k_1 P_1 H_e^+ - k_{-1} P_2 + k_{-2} P_3 - k_2 P_2 c_e \\
\frac{dP_3}{dt} &= k_2 P_2 c_e - k_{-2} P_3 + k_{-3} P_4 - k_3 P_3 \\
\frac{dP_4}{dt} &= k_3 P_3 - k_{-3} P_4 + k_{-4} P_5 c_{LS} - k_4 P_4 \\
\frac{dP_5}{dt} &= k_4 P_4 - k_{-4} P_5 c_{LS} + k_{-5} P_6 H_{LS}^+ - k_5 P_5 \\
\frac{dP_6}{dt} &= k_5 P_5 - k_{-5} P_6 H_{LS}^+ + k_{-6} P_1 - k_6 P_6
\end{aligned} \tag{14}$$

Additionally, the sum of all protein states must be equal to the total number of proteins (P_o) at a particular time

$$P_0 = P_1 + P_2 + P_3 + P_4 + P_5 + P_6 \tag{15}$$

In this study proteins are considered as not being actively added to the membrane; hence P_0 is a constant. At steady state, individual quantities of proteins can be solved from Eqs. (14) and (15). Since there are seven equations for six unknowns, not all equations are independent. Thus, they can be reorganized in a 6×6 matrix as

$$\begin{bmatrix}
1 & 1 & 1 & 1 & 1 & 1 \\
-k_{-6} - k_1 H_e^+ & k_{-1} & 0 & 0 & 0 & k_6 \\
k_1 H_e^+ & -k_{-1} - k_2 c_e & k_{-2} & 0 & 0 & 0 \\
0 & k_2 c_e & -k_{-2} - k_3 & k_{-3} & 0 & 0 \\
0 & 0 & k_3 & -k_{-3} - k_4 & k_{-4} c_{LS} & 0 \\
0 & 0 & 0 & k_4 & -k_{-4} c_{LS} - k_5 & k_{-5} H_{LS}^+
\end{bmatrix}
\begin{bmatrix} P_1 \\ P_2 \\ P_3 \\ P_4 \\ P_5 \\ P_6 \end{bmatrix}
=
\begin{bmatrix} P_0 \\ 0 \\ 0 \\ 0 \\ 0 \\ 0 \end{bmatrix} \tag{16}$$

The net transport of sucrose molecules inwards will be equal to the net rate at which sucrose leaves the protein on the internal site (see the process in Fig. 2(*d*)). Thus, the sucrose influx is

$$J_{\text{suc}} = k_4 P_4 - k_{-4} P_5 c_{\text{LS}} \tag{17}$$

By replacing the protein densities, the resulting sucrose flux can be represented as a function of leaf reactant concentrations and rate constants

$$J_{\text{suc}} = P_o \frac{H_e^+ c_e k_1 k_2 k_3 k_4 k_5 k_6 - H_{\text{LS}}^+ c_{\text{LS}} k_{-1} k_{-2} k_{-3} k_{-4} k_{-5} k_{-6}}{\Phi(k_m, k_{-m}, H_e^+, H_{\text{LS}}^+, c_e, c_{\text{LS}})} \tag{18}$$

Here the denominator Φ is composed of 36 terms

$$\begin{aligned}\Phi = {} & k_{-1}k_{-2}k_{-3}k_{-6}k_5 + k_{-1}k_{-2}k_{-3}k_5k_6 + k_{-1}k_{-2}k_{-6}k_4k_5 + k_{-1}k_{-2}k_4k_5k_6 + k_{-1}k_{-6}k_3k_4k_5 \\ & + k_{-1}k_3k_4k_5k_6 + H_{\text{LS}}^+k_{-1}k_{-2}k_{-3}k_{-5}k_{-6} + H_{\text{LS}}^+k_{-1}k_{-2}k_{-5}k_{-6}k_4 + H_e^+k_{-2}k_{-3}k_1k_5k_6 \\ & + H_{\text{LS}}^+k_{-1}k_{-5}k_{-6}k_3k_4 + H_e^+k_{-2}k_1k_4k_5k_6 + H_e^+k_1k_3k_4k_5k_6 + c_{\text{LS}}k_{-1}k_{-2}k_{-3}k_{-4}k_{-6} + c_{\text{LS}}k_{-1}k_{-2}k_{-3}k_{-4}k_6 \\ & + c_ek_{-6}k_2k_3k_4k_5 + c_ek_2k_3k_4k_5k_6 + H_{\text{LS}}^+c_{\text{LS}}k_{-1}k_{-2}k_{-3}k_{-4}k_{-5} + H_{\text{LS}}^+c_{\text{LS}}k_{-1}k_{-2}k_{-4}k_{-5}k_{-6} \\ & + H_{\text{LS}}^+c_{\text{LS}}k_{-1}k_{-3}k_{-4}k_{-5}k_{-6} + H_{\text{LS}}^+c_{\text{LS}}k_{-2}k_{-3}k_{-4}k_{-5}k_{-6} + H_e^+c_{\text{LS}}k_{-2}k_{-3}k_{-4}k_1k_6 + H_{\text{LS}}^+c_{\text{LS}}\text{k}_{-1}\text{k}_{-4}\text{k}_{-5}\text{k}_{-6}\text{k}_3 \\ & + H_e^+c_ek_{-3}k_1k_2k_5k_6 + H_{\text{LS}}^+c_ek_{-5}k_{-6}k_2k_3k_4 + H_e^+c_ek_1k_2k_3k_4k_5 + H_e^+c_ek_1k_2k_3k_4k_6 \\ & + H_e^+c_ek_1k_2k_3k_5k_6 + H_e^+c_ek_1k_2k_4k_5k_6 + H_e^+H_{\text{LS}}^+c_{\text{LS}}k_{-2}k_{-3}k_{-4}k_{-5}k_1 + H_e^+H_{LS}^+c_ek_{-5}k_1k_2k_3k_4 \\ & + H_{LS}^+c_ec_{\text{LS}}k_{-3}k_{-4}k_{-5}k_{-6}k_2 + H_e^+c_ec_{\text{LS}}k_{-3}k_{-4}k_1k_2k_6 + H_{LS}^+c_ec_{\text{LS}}k_{-4}k_{-5}k_{-6}k_2k_3 + H_e^+c_ec_{\text{LS}}k_{-4}k_1k_2k_3k_6 \\ & + H_e^+H_{\text{LS}}^+c_ec_{\text{LS}}k_{-3}k_{-4}k_{-5}k_1k_2 + H_e^+H_{\text{LS}}^+c_ec_{\text{LS}}k_{-4}k_{-5}k_1k_2k_3\end{aligned} \tag{19}$$

4 Numerical Method

In this study we have developed an in-house numerical model using the finite volume method [26,27] with collocated storage to study the physics of transport through petiole sieve tubes. The governing equations are discretized for 2D rectangular coordinates. The semi-implicit method for pressure-linked equations (SIMPLE) algorithm with collocated mesh is implemented. The governing equations are solved using the line-by-line tridiagonal matrix algorithm. Since we use an iterative solver, convergence of continuum variables is very important. At early iterations the solution easily diverges; therefore, a smaller relaxation coefficient is used. For later iterations divergence is less likely to occur; hence, larger relaxation coefficients can be used.

Sieve plates are incorporated by computational cell blocking. In the case of the Navier–Stokes equations, a large viscous term is used to block flow while for the Nernst–Planck equation a large diffusive term is used to block sucrose flux. Numerical results are obtained for the first four to six petiole sieve elements and the least squares method is used to extrapolate the results to the full petiole length (5 cm).

5 Model Parameters

5.1 Physical Properties. In our numerical simulations, petiole sieve tube dimensions are based on realistic plant values. Petiole sieve elements are modeled as rectangular channels 120 μm in length and 11 μm in height, based on the dimensions of tobacco sieve elements [28]. The sieve plate thickness is set as 1.2 μm. We consider pores as slits with a diameter of 0.69 μm. The companion cell to sieve tube height ratio α_{cc} is set at 70% [29]. The leaf sieve to petiole sieve length scale factor is estimated from the leaf companion cell surface area, leaf vein density, and stem sieve tubes resulting in a factor of $\alpha = 10$. The leaf companion cell to sieve conversion factor is estimated using leaf companion cell values, giving an estimate of $\alpha_{\text{ccL}} = 8.95$. The dimensions of the plasmodesmata are taken from plant roots [30], where the length is 147 nm, the inner radius is 3.6 nm, and the outer radius is 7.6 nm (based on gap estimates). The plasmodesmata density is set as 10 μm^{-2} from the ranges of plasmodesmata density in plants.

5.2 Fluid Properties. A sucrose-water solution is considered as the fluid in this study. Over the simulated sucrose concentration range, the actual fluid density change is less than 4%, thus incompressibility is a reasonable assumption. We set the fluid density as 1090 kg/m^3 based on a 700 mM sucrose solution at 25 °C. However the fluid viscosity, diffusivity, and osmotic pressure are strong functions of sucrose concentration. The fluid viscosity μ is calculated from Chenlo et al. [31]

$$\mu = 890.5 \times 10^{-6}(1 + 0.867c)^{0.164}\left[1 + 0.73c\exp\left(0.4843\, c^{1.1}\right)\right] \quad \text{for } c \le 4.5\, m \tag{20}$$

The sucrose diffusivity D is estimated by applying an exponential fit to data from Ekdawi et al. [32] and Chatterjee [33]

$$D = 5.23 \times 10^{-10}\exp(-0.7248c) \quad \text{for } c \le 8.3\, m \tag{21}$$

The osmotic pressure π is calculated using the equation given by Michel [34]

$$\pi = RT\rho_{\text{water}}\left(0.998c + 0.089c^2\right) \quad \text{for } 0.1 \le c \le 1.0\, m \tag{22}$$

The density of pure water (ρ_{water}) at 25 °C is considered in this study to calculate osmotic pressure. The apoplast thermodynamic pressure is considered as zero with the apoplast osmotic pressure at the leaf (π_e^{leaf}) and stem (π_e^{stem}) as 0.7 MPa and 0.3 MPa, respectively, based on measured water potentials for tobacco plants [35]. In addition, we assume a linear change in osmotic pressure between the leaf and stem, as shown in Fig. 1(*b*).

5.3 Chemical Properties. To find the inlet boundary condition for fluid flow, the sucrose influx should be known. In Sec. 3, we have provided a model to estimate the sucrose flux in terms of reaction rate constants. For our simulation we selected rate constants (see Table 1) from Boorer et al. [17] with modifications made to k_{-4} and k_{-5} to account for the dependency on the leaf sieve proton and sucrose concentration. Rate k_{-5} is modified for 1st order dependency to include the leaf sieve proton concentration by using oocyte pH. In addition, k_{-4} is estimated by considering the chemical equilibrium condition with no sucrose flux.

Table 1 Selected rate constants for six-state model for potato plant proton sucrose transporter [17]. Rate k_5 is varied in certain simulations.

Forward reaction	Rate	Units	Reverse reaction	Rate	Units
k^*_1	7.0×10^7	$M^{-1}\,s^{-1}$	k^*_{-1}	2.3×10^2	s^{-1}
k_2	1.7×10^3	$M^{-1}\,s^{-1}$	k_{-2}	5.0	s^{-1}
k_3	50	s^{-1}	k_{-3}	50	s^{-1}
k_4	1.0×10^3	s^{-1}	k_{-4}	3.79×10^2	$M^{-1}\,s^{-1}$
k_5	4.3	s^{-1}	k_{-5}	1.41×10^9	$M^{-1}\,s^{-1}$
k^*_6	6.0	s^{-1}	k^*_{-6}	5.0	s^{-1}

Table 2 Grid refinement analysis results with respect to the finest grid (120 × 128)

Grid setup	u error (%)	v error (%)	p error (%)	c error (%)
30×32	0.1766	0.4474	4.153×10^{-7}	8.101×10^{-4}
60×64	0.0270	0.0823	3.077×10^{-8}	4.882×10^{-5}

While the rate constants for the reactions in Figs 2(*b*)–2(*e*) are known, the rate constants for reactions in Figs. 2(*a*) and 2(*f*) (k_1, k_{-1}, k_6, k_{-6}) are dependent on membrane electric potential. The rates for potential dependent steps (k^*_1, k^*_{-1}, k^*_6, and k^*_{-6}) are given as [17]

$$k_{\pm} = k^*_{\pm} \exp(\mp 0.5\,\delta F V_m / RT) \tag{23}$$

where V_m is the membrane electrical potential difference, δ is the fraction of the electric field sensed by the process in Figs. 2(*a*) and 2(*f*). For the reactions in Figs. 2(*a*) and 2(*f*), δ is given as 0.4 and 0.6, respectively.

6 Error Analysis

The grid dependency is tested by simulating for 30×32, 60×64, and 120×128 computational cells per sieve element with a 600 mM leaf sieve sucrose concentration, 60×10^{-14} m/Pa s cell membrane permeability, and 1 MPa outlet thermodynamic pressure. To better model the sieve plate, an adaptive mesh is used with finer grids near the sieve plate. On the contrary, a uniform grid size is used in the y direction for consistent pore sizing. Simulation results for different grid numbers per sieve element are compared to verify the grid independency. The sucrose concentration, pressure, and velocity for coarser grids are compared with the finest case at $x = 399\ \mu$m and $y = 5.5\ \mu$m. The results for the relative errors are listed in Table 2. These errors are within a reasonable value and the finest grid size is used for the simulations.

7 Results and Discussion

Numerical simulations are presented based on the plant properties as described in Sec. 5. Typical sieve tube pressures may range from 0.8 to 1.4 MPa; thus, we consider a petiole sieve outlet pressure of 1 MPa. Membrane permeability is based on Arabidopsis leaf cell plasma membranes and set as 60×10^{-14} m/Pa s [36]. To calculate the sucrose flux for the inlet flow velocity, the properties including proton and sucrose concentrations, electric potentials,

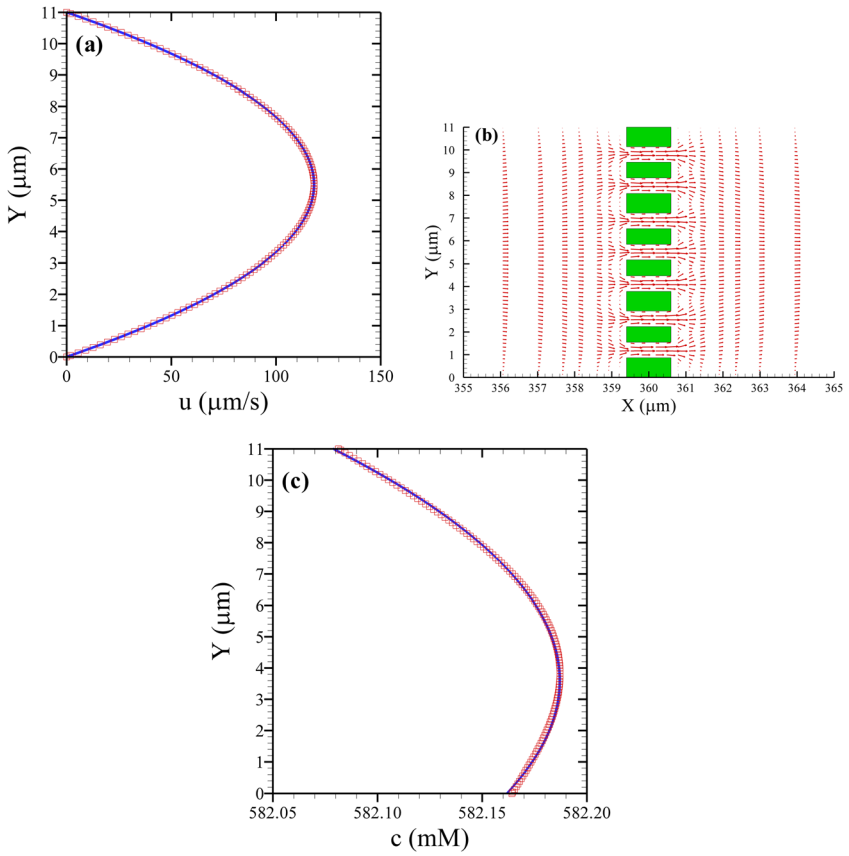

Fig. 3 (*a*) Cross-stream (y) distributions far away from sieve plates for the u-velocity. (*b*) Vector plot for fluid flow past simulated sieve plate. (*c*) Cross-stream (y) distributions far away from sieve plates for petiole sieve sucrose concentration. In figures (*a*) and (*c*) the open circles are data points from simulations taken at $x = 400\ \mu$m and the solid lines are parabolic curve fits.

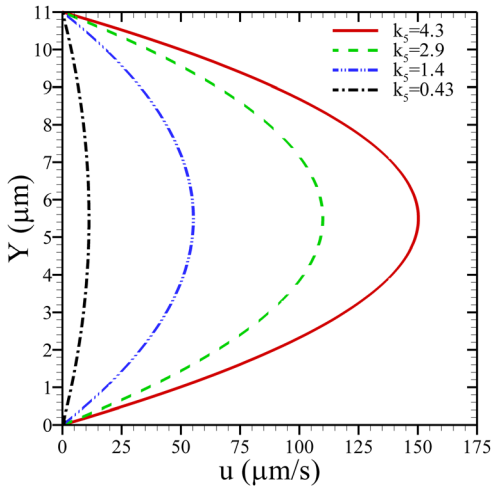

Fig. 4 Outflow velocity distribution for different proton dissociation rate constants k_5 in units of s^{-1}. All other simulation conditions are the same as in Fig. 3.

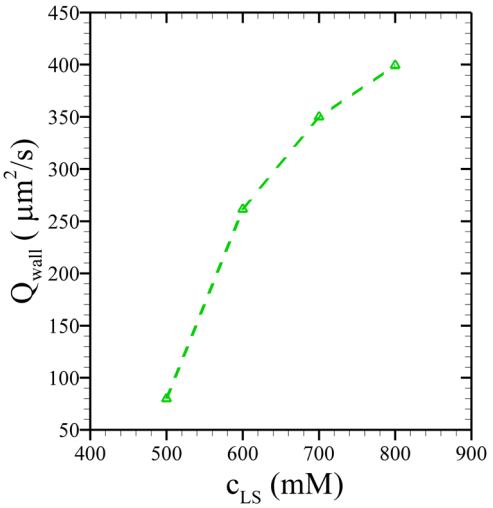

Fig. 6 Petiole sieve tube wall inflow for different leaf sieve tube sucrose concentrations c_{LS}. All other simulation conditions are the same as in Fig. 3. Here Q_{wall} is the wall volumetric flow rate per unit depth.

and protein (STP) densities need to be defined. Reactant concentrations in the apoplast surrounding the leaf sieve tube are defined based on potato plants with a *p*H of 6.1 [37] and a sucrose concentration of 2.1 mM [38]. The leaf sieve *p*H and membrane electrical potential difference are chosen as 7.5 and −140 mV, respectively [39]. A negative membrane electrical potential implies a more negative voltage on the inside of the leaf sieve compared to the surrounding apoplast. We use an STP density of 0.12 proteins nm^{-2} based on estimates of companion cell sucrose fluxes.

7.1 Flow and Concentration Field in Sieve Tube. Figure 3 shows the numerical results in the petiole sieve tube for a leaf sieve sucrose concentration (c_{LS}) of 600 mM and k_5 of 4.3 s^{-1}. The streamwise velocity distribution far away from a sieve plate is shown in Fig. 3(*a*). The flow distribution closely follows a parabolic profile due to the low Reynolds numbers ($Re = 4 \times 10^{-4}$ to 3×10^{-3}) in the microscale sieve tube. The flow field distribution around a sieve plate is shown in Fig. 3(*b*). Again, due to the low Reynolds number, the velocity quickly approaches parabolic. The flow will be distorted as it approaches the sieve plates. Once inside the sieve pores, the flow quickly becomes a parabolic profile with similar velocities at different positioned pores. Flow field in sieve pores will be similar because the pores are similarly sized, uniformly spaced, and located in parallel. Soon after passing the sieve plates, again, due to the low Reynolds number, the overall flow becomes a parabolic profile with no noticeable fluid circulation.

The sucrose concentration distribution at $x = 400\,\mu$m is illustrated in Fig. 3(*c*). The resulting sucrose concentration distribution can be closely approximated by a parabolic profile. Due to wall inflow, the sugar concentration near the wall will be slightly lower; hence, the higher sucrose concentration will occur near the center. In the case of our simulation domain, due to the companion cells being on the top half, more the wall inflow will occur on the upper side; hence, the sucrose concentration profile is asymmetrical. Nevertheless, considering the very small change in the sucrose concentration across the channel, the sugar concentration could be assumed uniform along the *y*-direction.

7.2 Sucrose Transporter Dependency. To understand how the sucrose transporter protein alters active pumping through the petiole sieve tube, we vary the rate constants. Based on rate constant orders, the value of k_5 is varied. The rate constant k_5 is related to the proton dissociation step (see Fig. 2(*e*)), where increasing this value means protons will leave the transporter more freely on the leaf sieve side. Figure 4 shows the outflow velocity distribution for different rates of k_5. Increasing the forward rate constant implies accelerating the forward reaction, which will

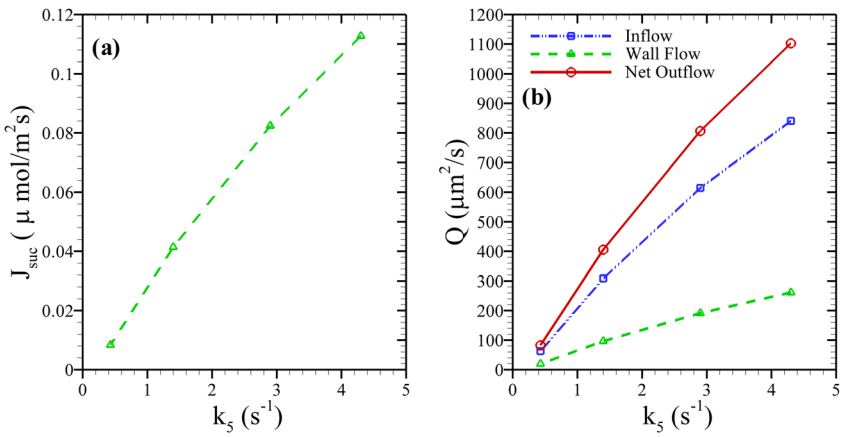

Fig. 5 Effects of the proton dissociation rate constant k_5 on (*a*) sucrose influx, and (*b*) sieve tube inflow, wall flow, and total outflow. All other simulation conditions are the same as in Fig. 3. Here Q is the volumetric flow per unit depth.

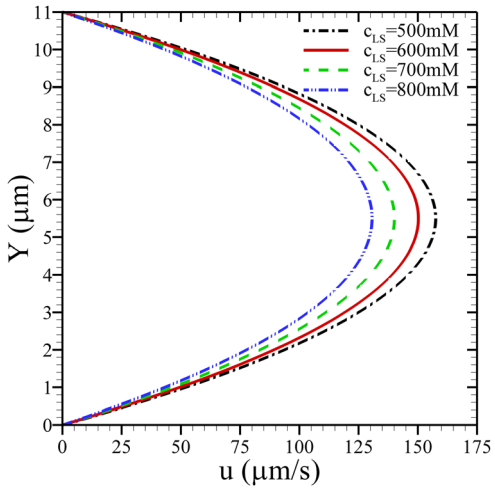

Fig. 7 Velocity distribution at the outlet for different leaf sieve tube sucrose concentrations c_{LS}

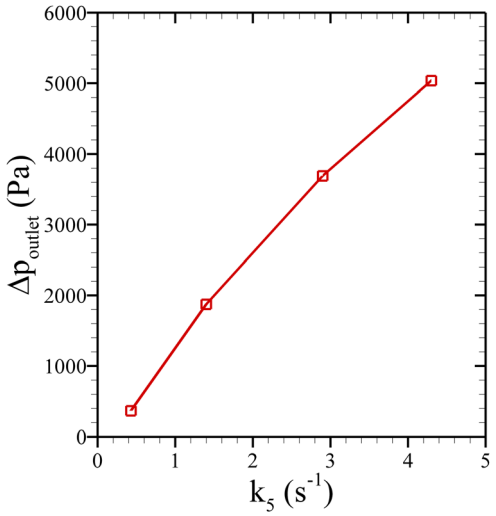

Fig. 8 Effect of sieve plates on flow through the petiole sieve tube. The outlet pressure difference between without and with sieve plates for different proton dissociation rate constants k_5, is shown. All other simulation conditions are the same as in Fig. 3.

increase the quantity of sucrose entering the petiole sieve tube. This sucrose influx increase will result in more sucrose molecules to drive a larger flow through the tube; hence, the overall flow velocity will increase.

Figure 5(*a*) shows the sucrose influx for different k_5. The sucrose flux first rapidly increases and then the increase slows down at higher k_5. This is due to the fact that as the forward reaction (see Fig. 2(*e*)) becomes faster, the rate of the overall sucrose transport process will be more and more limited by other steps. In Fig. 5(*b*) we compare the inflow and wall flow with total outflow for different values of the rate constant k_5. The inflow follows the same trend as the sucrose flux for a given leaf sucrose concentration because of the linear relationship presented in Eq. (12). Similar to the inflow and sucrose flux, the wall flow also increases with an increase in the reaction rate constants. This is due to the fact that more sucrose molecules will drive more water molecules through the wall at higher value of k_5. Figure 5(*b*) shows that the wall flow is much smaller than the inflow at the petiole tube. For the case presented in this study, the wall flow is more than three times smaller than the inflow. The value of the wall flow can be increased or decreased by other parameters such as the leaf sieve sucrose concentration. Nevertheless, the wall flow is on the same order of magnitude of the inflow, indicating the osmotic pumping through the petiole tube.

7.3 Leaf Sieve Sugar Concentration Dependency. In this section, the leaf sieve sugar concentration c_{LS} is varied based on known sucrose concentration ranges. We simulate the petiole sieve tube for a forward rate constant k_5 of 4.3 s^{-1}. In our simulations, the leaf sieve sucrose concentration is used as the input concentration for the petiole tube. Figure 6 shows that the wall inflow increases with the leaf sieve sucrose concentration. This is due to the fact that as the sucrose concentration increases in the petiole tube, the osmotic pressure will increase, driving a larger flow from the apoplast to the sieve tube through the wall membrane. However, the effect of the leaf sucrose concentration on the inflow is opposite. As the leaf sucrose concentration increases, the inflow decreases due to two reasons. First, for a fixed sucrose flux, a higher leaf sieve sucrose concentration will mean that there will be less water inflow. Second, the STP moves sucrose from low (apoplast) to high sugar concentration (leaf sieve); hence, a higher leaf sieve sucrose concentration will mean that sucrose transport will be difficult. In other words, the water inflow will be increased as the leaf sieve sucrose concentration is decreased. The benefit of increased inflow outweighs the reduction in wall flow for a lower value of the leaf sieve sucrose concentration. Therefore, the outflow is higher for lower leaf sieve sugar concentrations, as shown in Fig. 7.

7.4 Sieve Plate Dependency. In microfluidic devices, the minimization of frictional resistance is desired. Thus, it is important to understand the transport behavior in sieve tubes in the absence of sieve plates. We have specifically studied the effect of rate constants in the flow performance of the petiole sieve tube without sieve plates, where we compare the results with the case including sieve plates. To simulate the dependency on sieve plates, the leaf sieve sugar concentration is set as 600 mM. Simulations are performed with same inlet pressure for comparing cases with and without sieve plates. Shown in Fig. 8 is the difference in the outlet thermodynamic pressure ($\Delta p_{outlet} = p_{outlet}^{without} - p_{outlet}^{with}$) for a different reaction rate constant k_5. Since the inlet pressures are equal, the difference in outlet pressure shows the pressure gained due to the removal of sieve plates. Without sieve plates, the outlet pressure is much higher than with sieve plates due to less restriction in the flow. In other words, for a similar rate constant and leaf sieve pressure, water can be transported for a longer distance without sieve plates.

8 Conclusions

A cellular level phloem model for studying water and sucrose transport through petiole sieve tubes is developed considering plant active loading mechanisms. The main feature of this phloem model is the incorporation of proton sucrose transporter kinetics (active loading) through the use of a six-state model based on potato sucrose transporter proteins. This model allows us to investigate the impacts of a wide range of physical and biochemical parameters on the sucrose transport in plants. Governing equations, including the Nernst–Planck, Navier–Stokes, and continuity equations are solved for 2D flows using the finite volume method. The governing equations are discretized and solved using the SIMPLE algorithm for collocated storage. Based on the grid independent study when 120×128 grid points are used per sieve element, the errors including sucrose concentration, pressure, and velocity are within reasonable value. Due to the computational expense, fewer sieve elements are modeled and an extrapolation technique is used to obtain results for the flow through a petiole sieve tube.

This numerical model indicates that the spatial variation for velocity is parabolic, both in the sieve tube and inside the pores of sieve plates. However, the spatial variation is negligible for the sucrose concentration. The sucrose concentration distribution is asymmetric due to the unequal value of wall inflow from the top

and bottom walls. The influence of the proton sucrose transport mechanics on the petiole sieve tube is studied by altering the internal (sieve side) proton dissociation rate constant k_5. The numerical results indicate that accelerating forward reactions in the transporter protein significantly increases sucrose influx. This increase in sucrose flux significantly increases both the inflow and wall inflow, leading to a net increase in outflow.

In addition, we consider the influence of altering leaf sieve sucrose concentrations on transport through petiole sieve tubes. From our numerical results, a smaller leaf sieve sucrose concentration results in higher outflow. Over the petiole sieve region, wall inflow is smaller with lower leaf sieve sucrose concentrations. However, a lower leaf sieve sucrose concentration allows the sucrose transporter to move more sucrose molecules, resulting in larger inflow outweighing the reduction in wall flow and, hence, larger outflow.

Acknowledgment

This work was supported in part by the National Science Foundation under Grant No. CBET 1250107.

Nomenclature

c = sucrose concentration in petiole sieve, mM
c_e = sucrose concentration in apoplast (surrounding sieve), mM
c_{LS} = sucrose concentration inside of leaf sieve, mM
d_{Pore} = sieve plate pore diameter, m
D = sucrose diffusivity, m^2/s
F = Faraday's constant, C/mol
h = sieve tube height, m
H^+ = proton concentration, mM
ϑ_{pl} = plasmodesmata density, no./m^2
J_{suc} = sucrose influx, mol/m^2 s
k_m = mth rate constant
L = petiole length, m
L_{pl} = plasmodesmata length, m
L_{plate} = sieve plate thickness, m
L_{SE} = sieve element length, m
M_p = cell membrane hydraulic permeability, m/Pa s
p = thermodynamic pressure, Pa
P_m = mth sucrose transporter protein density, #/m^2
P_0 = total sucrose transporter protein density, no./m^2
q = volume flow rate, m^3/s
Q = volume flow rate per unit width, m^2/s
r_{pl} = plasmodesmata radius, m
R = ideal gas constant, J/mol K
T = absolute temperature, K
u = streamwise flow velocity, m/s
v = cross-stream flow velocity, m/s
V_m = membrane electrical potential difference, V
x = position along the sieve tube, m
y = position across the sieve tube, m
α = sieve tube leaf to petiole length ratio c_e
α_{cc} = companion cell to sieve height ratio
α_{ccL} = leaf companion cell surface area to sieve wall area ratio
δ = fraction of electric field sensed
μ = dynamic viscosity, Pa s
π = osmotic pressure in the petiole sieve, Pa
π_e = osmotic pressure in the apoplast (surrounding sieve), Pa
ρ = fluid density, kg/m^3
σ = membrane reflection coefficient

References

[1] Yairi, M. and Richter, C., 2007, "Massively Parallel Microfluidic Pump," Sens. Actuators, A, **137**(2), pp. 350–356.
[2] Schroeder, M. A., Salloum, K. S., Perbost, M., Lebl, M., and Posner, J. D., 2011, "Radial Flow Electroosmotic Pump," Sens. Actuators, A, **169**(1), pp. 250–255.
[3] Shim, J. and Dutta, P., 2012, "Joule Heating Effect in Constant Voltage Mode Isotachophoresis in a Microchannel," Int. J. Nonlinear Sci. Numer. Simul., **13**(5), pp. 333–344.
[4] Horiuchi, K., Dutta, P., and Hossain, A., 2006, "Joule-Heating Effects in Mixed Electro-Osmotic and Pressure-Driven Microflows Under Constant Wall Heat Flux," J. Eng. Math., **54**(2), pp. 159–180.
[5] Pal, S., Datta, A., Sen, S., Mukhopdhyay, A., Bandopadhyay, K., and Ganguly, R., 2011, "Characterization of a Ferrofluid-Based Thermomagnetic Pump for Microfluidic Applications," J. Magn. Magn. Mater., **323**(21), pp. 2701–2709.
[6] Li, G., Luo, Y., Chen, Q., Liao, L., and Zhao, J., 2012, "A"Place n Play"Modular Pump for Portable Microfluidic Applications," Biomicrofluidics, **6**(1), p. 014118.
[7] Squires, T. M., 2010, "A Furtive Stare at an Intra-Cellular Flow," J. Fluid Mech, **642**(01), pp. 1–4.
[8] Sundaresan, V. B. and Leo, D. J., 2008, "Modeling and Characterization of a Chemomechanical Actuator Using Protein Transporter," Sens. Actuators B, **131**(2), pp. 384–393.
[9] Daudet, F. A., Lacointe, A., Gaudillère, J. P., and Cruiziat, P., 2002, "Generalized Münch Coupling Between Sugar and Water Fluxes for Modelling Carbon Allocation as Affected by Water Status," J. Theor. Biol., **214**(3), pp. 481–498.
[10] De Schepper, V. and Steppe, K., 2010, "Development and Verification of a Water and Sugar Transport Model Using Measured Stem Diameter Variations," J. Exp. Bot., **61**(8), pp. 2083–2099.
[11] Thompson, M. V. and Holbrook, N. M., 2003, "Application of a Single-Solute Non-Steady-State Phloem Model to the Study of Long-Distance Assimilate Transport," J. Theor. Biol., **220**(4), pp. 419–455.
[12] Christy, A. L. and Ferrier. J. M., 1973, "A Mathematical Treatment of Munch's Pressure-Flow Hypothesis of Phloem Translocation," Plant Physiol., **52**(6), pp. 531–538.
[13] Schulte, P. J., 1999, "Water Flow Through a 20-Pore Perforation Plate in Vessels of Liquidambar Styraciflua," J. Exp. Bot., **50**(336), pp. 1179–1187.
[14] Jensen, K. H., Mullendore, D. L., Holbrook, N. M., Bohr, T., Knoblauch, M., and Bruus, H., 2012, "Modeling the Hydrodynamics of Phloem Sieve Plates," Front. Plant Sci., **3**(151), pp. 1–11.
[15] Turgeon, R., 2010, "The Role of Phloem Loading Reconsidered," Plant Physiol., **152**(4), pp. 1817–1823.
[16] Borstlap, A. C. and Schuurmans, J.A.M.J., 2004, "Sucrose Transport Into Plasma Membrane Vesicles From Tobacco Leaves by H+ Symport or Counter Exchange Does not Display a Linear Component," J. Membr. Biol., **198**(1), pp. 31–42.
[17] Boorer, K. J., Loo, D. D., Frommer, W. B., and Wright, E. M., 1996, "Transport Mechanism of the Cloned Potato H+/Sucrose Cotransporter StSUT1," J. Biol. Chem., **271**(41), pp. 25139–25144.
[18] Gomes, D., Agasse, A., Thiébaud, P., Delrot, S., Gerós, H., and Chaumont, F., 2009, "Aquaporins are Multifunctional Water and Solute Transporters Highly Divergent in Living Organisms," Biochim. Biophys. Acta, **1788**(6), pp. 1213–1228.
[19] Wu, F. and Tanksley, S. D., 2010, "Chromosomal Evolution in the Plant Family Solanaceae," BMC Genomics, **11**, p. 182.
[20] Sprague, I. B. and Dutta, P., 2011, "Modeling of Diffuse Charge Effects in a Microfluidic Based Laminar Flow Fuel Cell," Numer. Heat Transfer, Part A, **59**(1), pp. 1–27.
[21] Thompson, G. A. and Van Bel, A. J. E., 2013, *Phloem Molecular Cell Biology, Systemic Communication, Biotic Interactions*, Wiley-Blackwell, Ames, IA.
[22] Kargol, M. and Kargol, A., 2003, "Mechanistic Equations for Membrane Substance Transport and Their Identity With Kedem-Katchalsky Equations," Biophys. Chem., **103**(2), pp. 117–127.
[23] Bird, R. B., Stewart, W. E., and Lightfoot, E. N., 2002, *Transport Phenomena*, John Wiley and Sons, New York.
[24] Fu, Q., Cheng, L., Guo, Y., and Turgeon, R., 2011, "Phloem Loading Strategies and Water Relations in Trees and Herbaceous Plants," Plant Physiol., **157**(3), pp. 1518–1527.
[25] Zhou, J., Theodoulou, F., Sauer, N., Sanders, D., and Miller, A. J., 1997, "A Kinetic Model With Ordered Cytoplasmic Dissociation for SUC1, an Arabidopsis H+/Sucrose Cotransporter Expressed in Xenopus Oocytes," J. Membr. Biol., **159**(2), pp. 113–125.
[26] Shim, J., Dutta, P., and Ivory, C. F., 2007, "Finite-Volume Methods for Isotachophoretic Separation in Microchannels," Numer. Heat Transfer, Part A, **52**(5), pp. 441–461.
[27] Shim, J., Dutta, P., and Ivory, C. F., 2007, "Modeling and Simulation of IEF in 2-D Microgeometries," Electrophoresis, **28**(4), pp. 572–586.
[28] Mullendore, D. L., Windt, C. W., Van As, H., and Knoblauch, M., 2010, "Sieve Tube Geometry in Relation to Phloem Flow," Plant Cell, **22**(3), pp. 579–593.
[29] Kempers, R., Ammerlaan, A., and Van Bel, A. J. E., 1998, "Symplasmic Constriction and Ultrastructural Features of the Sieve Element/Companion Cell Complex in the Transport Phloem of Apoplasmically and Symplasmically Phloem-Loading Species," Plant Physiol., **116**(1), pp. 271–278.
[30] Overall, R. L., Wolfe, J., and Gunning, B. E. S., 1982, "Intercellular Communication in Azolla Roots: I. Ultrastructure of Plasmodesmata," Protoplasma, **111**(2), pp. 134–150.
[31] Chenlo, F., Moreira, R., Pereira, G., and Ampudia, A., 2002, "Viscosities of Aqueous Solutions of Sucrose and Sodium Chloride of Interest in Osmotic Dehydration Processes," J. Food Eng., **54**(4), pp. 347–352.
[32] Ekdawi-Sever, N., de Pablo, J. J., Feick, E., and von Meerwall, E., 2003, "Diffusion of Sucrose and Alpha, Alpha-Trehalose in Aqueous Solutions," J. Phys. Chem. A, **107**, pp. 936–943.

[33] Chatterjee, A., 1964, "Measurement of the Diffusion Coefficients of Sucrose in Very Dilute Aqueous Solutions Using Jamin Interference Optics at 25 deg," J. Am. Chem. Soc., **86**(5), pp. 793–795.
[34] Michel, B. E., 1972, "Solute Potentials of Sucrose Solutions," Plant Physiol., **50**(1), pp. 196–198.
[35] Begg, J. E. and Turner, N. C., 1970, "Water Potential Gradients in Field Tobacco," Plant Physiol., **46**(2), pp. 343–346.
[36] Martre, P., Morillon, R., Barrieu, F., North, G. B., Nobel, P. S., and Chrispeels, M. J., 2002, "Plasma Membrane Aquaporins Play a Significant Role During Recovery From Water Deficit," Plant Physiol., **130**(4), pp. 2101–2110.
[37] Oja, V., Savchenko, G., Jakob, B., and Heber, U., 1999, "*p*H and Buffer Capacities of Apoplastic and Cytoplasmic Cell Compartments in Leaves," Planta, **209**(2), pp. 239–249.
[38] Sweetlove, L. J., Kossmann, J., Riesmeier, J. W., Trethewey, R. N., and Hill, S. A., 1998, "The Control of Source to Sink Carbon Flux During Tuber Development in Potato," Plant J., **15**(5), pp. 697–706.
[39] Hafke, J. B., van Amerongen, J. K., Kelling, F., Furch, A. C., Gaupels, F., and van Bel, A. J. E., 2005, "Thermodynamic Battle for Photosynthate Acquisition Between Sieve Tubes and Adjoining Parenchyma in Transport Phloem," Plant Physiol., **138**(3), pp. 1527–1537.